

# SLO-2 isoforms with unique Ca<sup>2+</sup>- and voltage-dependence characteristics confer sensitivity to hypoxia in *C. elegans*

Zhe Zhang,<sup>1,\*</sup> Qiong-Yao Tang,<sup>1</sup> Joseph T. Alaimo,<sup>2</sup> Andrew G. Davies,<sup>2</sup> Jill C. Bettinger<sup>2</sup> and Diomedes E. Logothetis<sup>1,\*</sup>

<sup>1</sup>Department of Physiology and Biophysics; Virginia Commonwealth University; Medical College of Virginia Campus; Richmond, VA USA;

<sup>2</sup>Department of Pharmacology and Toxicology; Virginia Commonwealth University; Medical College of Virginia Campus; Richmond, VA USA

**Keywords:** allosteric regulation, ion channels, membrane function, polymerase chain reaction (PCR), protein metal ion interaction, Ca<sup>2+</sup> binding, Slo channel

Slo channels are large conductance K<sup>+</sup> channels that display marked differences in their gating by intracellular ions. Among them, the Slo1 and *C. elegans* SLO-2 channels are gated by calcium (Ca<sup>2+</sup>), while mammalian Slo2 channels are activated by both sodium (Na<sup>+</sup>) and chloride (Cl<sup>-</sup>). Here, we report that SLO-2 channels, SLO-2a and a novel N-terminal variant isoform, SLO-2b, are activated by Ca<sup>2+</sup> and voltage, but in contrast to previous reports they do not exhibit Cl<sup>-</sup> sensitivity. Most importantly, SLO-2 provides a unique case in the Slo family for sensing Ca<sup>2+</sup> with the high-affinity Ca<sup>2+</sup> regulatory site in the RCK1 but not the RCK2 domain, formed through interactions with residues E319 and E487 (that correspond to D362 and E535 of Slo1, respectively). The SLO-2 RCK2 domain lacks the Ca<sup>2+</sup> bowl structure and shows minimal Ca<sup>2+</sup> dependence. In addition, in contrast to SLO-1, SLO-2 loss-of-function mutants confer resistance to hypoxia in *C. elegans*. Thus, the *C. elegans* SLO-2 channels possess unique biophysical and functional properties.

## Introduction

The BK (Maxi K, Slo) potassium channel family includes Slo1, Slo2 and Slo3 as its members. Among them, the Slo1 channel is gated by Ca<sup>2+</sup>,<sup>1,2</sup> while the Slo3 channel is activated by alkalization.<sup>3,4</sup> Slo2 channel gating exhibits species differences; the rat Slo2.2 (rSlo2.2 or Slack) and human Slo2.1 (hSlo2.1 or Slick) channels are each activated by both Na<sup>+</sup> and Cl<sup>-</sup>,<sup>5,6</sup> whereas the *C. elegans* Slo2a (SLO-2a) has been reported to be sensitive to Ca<sup>2+</sup> and Cl<sup>-</sup>.<sup>7</sup> Based on structure and sequence alignment, the C-termini of Slo1 channels are organized into two functional RCK (regulation of conductance for K) domains, RCK1 and RCK2. Three distinct Ca<sup>2+</sup> binding sites, two high-affinity and one low-affinity sites, have been reported in Slo1 C-termini based on electrophysiological experiments. One of the high-affinity Ca<sup>2+</sup> binding sites, located in the RCK2 domain, is composed of five consecutive Asp amino acid residues and referred to as the “Ca<sup>2+</sup> bowl.”<sup>8</sup> The second high-affinity Ca<sup>2+</sup> binding site located predominantly in the RCK1 domain involves residues D367 and E535.<sup>9</sup> A crystal structure of the C-terminus of Slo1 channels in the presence of Ca<sup>2+</sup>, consistent with electrophysiological data, identified the oxygen atoms of the side-chain carboxylate groups of D895 and D897 and the main-chain carbonyl oxygens of Q889 and D892 as the Ca<sup>2+</sup> coordination site.<sup>10</sup> This study did not resolve a Ca<sup>2+</sup> ion bound in the RCK1 domain, and the D367-E535 were

positioned in such a way that could not possibly coordinate a Ca<sup>2+</sup> ion. Another crystal structure of the C-terminus of Slo1, in the absence of Ca<sup>2+</sup>, localized the oxygen atoms of the RCK1 D367 in close proximity to the side chain carboxylate group of E535, consistent with experimental data implicating these residues as part of a high-affinity Ca<sup>2+</sup> coordination site.<sup>11,12</sup> However, this RCK1 Ca<sup>2+</sup> binding site has not been structurally shown yet in complex with Ca<sup>2+</sup>. Similarly, this crystal structure determined in the absence of divalents localized the E374/E399 site, which has displayed low affinity to Ca<sup>2+</sup>, Mg<sup>2+</sup> and Zn<sup>2+</sup>, on the upper plateau of the gating ring and close to the membrane. Biochemical data have raised the possibility that RCK1 may only serve to transduce Ca<sup>2+</sup> binding into a structural rearrangement.<sup>13</sup>

Unlike the mammalian Slo1 channel, it remains unclear how *C. elegans* SLO-2 channels sense Ca<sup>2+</sup>. Moreover, SLO-2 channels have been reported to sense Cl<sup>-</sup> ions, like their mammalian counterparts that sense Cl<sup>-</sup> and Na<sup>+</sup> ions. For Slo2.2 channels, we have previously reported that the side chains of D818 and H823 in the RCK2 domain are critical for Na<sup>+</sup> coordination and channel activation.<sup>14</sup> The Cl<sup>-</sup> coordination sites remain unknown. Loss-of-function studies of SLO-2 in *C. elegans* have been reported to cause hypersensitivity to hypoxia.<sup>5</sup>

Here we cloned and characterized a novel isoform of the *C. elegans* Slo2 channel, SLO-2b. We demonstrated that both SLO-2a and SLO-2b can be activated by Ca<sup>2+</sup> but not by Cl<sup>-</sup>,

\*Correspondence to: Zhe Zhang; Email: zzhang5@vcu.edu; Diomedes E. Logothetis; Email: delogothetis@vcu.edu

Submitted: 03/08/13; Revised: 03/27/13; Accepted: 03/28/13

<http://dx.doi.org/10.4161/chan.24492>

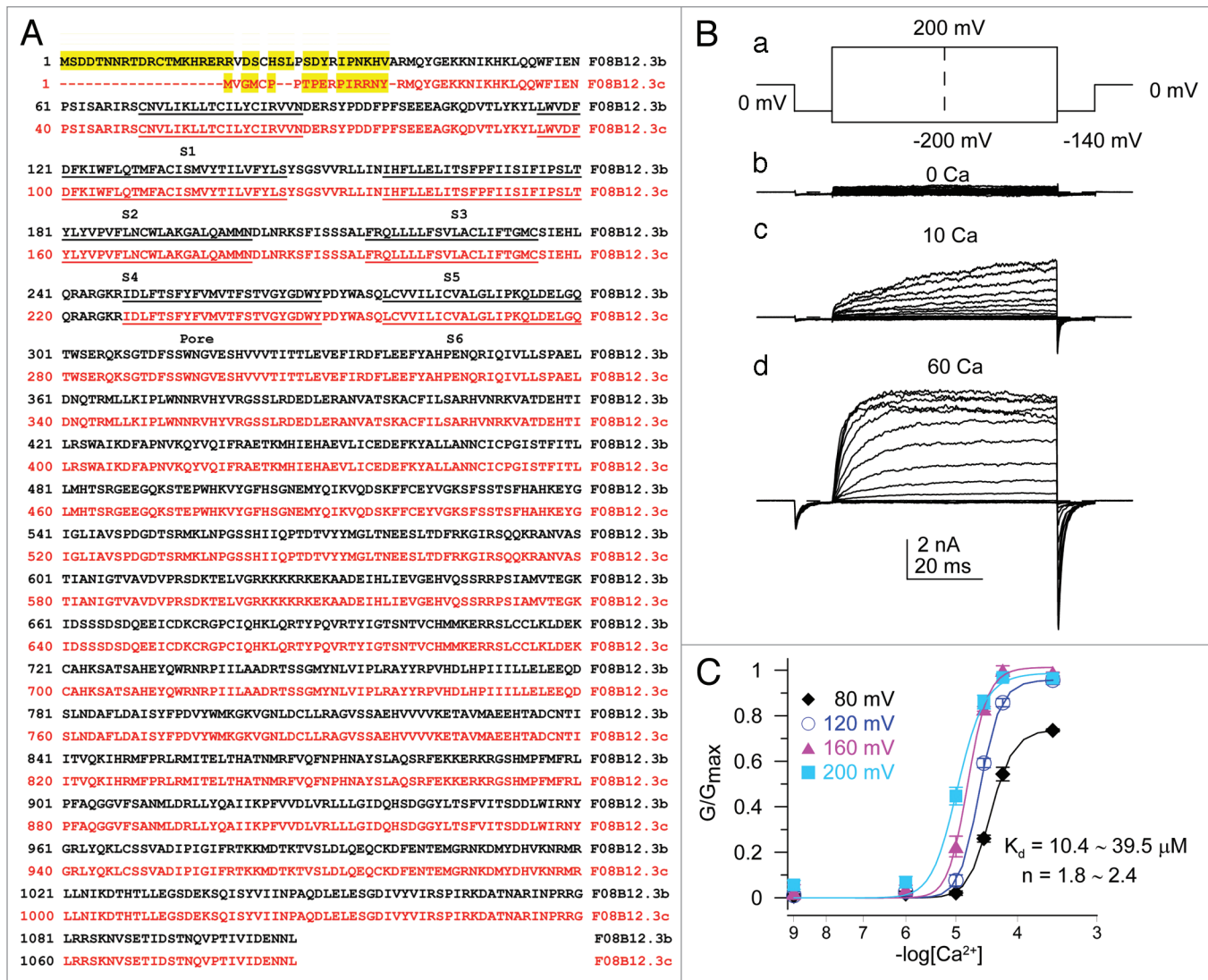


**Figure 1.** Amino acid sequence of the *C. elegans* SLO-2b channel and  $\text{Ca}^{2+}$  dependence of its macroscopic conductance. (A) The full amino acid sequences of SLO-2b (in red, F08B12.3c) and SLO-2a (in black, F08B12.3b). (B) Current traces of inside-out macropatches expressing SLO-2b, bathed in the indicated  $\text{Ca}^{2+}$  concentrations. Pipette Solution: 140 mM KMES (potassium methanesulphonate), 20 mM KOH, 10 mM HEPES, 2 mM  $\text{MgCl}_2$  (pH 7.0). The bath solution used in inside-out patch recordings contained 140 mM KMES, 20 mM KOH, 10 mM HEPES and one of the following: 5 mM EGTA (for nominally 0  $\text{Ca}^{2+}$ , 1  $\mu\text{M}$   $\text{Ca}^{2+}$ ), 5 mM HEDTA (for 10  $\mu\text{M}$   $\text{Ca}^{2+}$  solutions) or no added  $\text{Ca}^{2+}$  buffer for 60  $\mu\text{M}$  and higher  $\text{Ca}^{2+}$ . (C) The normalized conductance is plotted as a function of  $[\text{Ca}^{2+}]$  for a range of command potentials. Solid lines show the best fits of the conductance at each voltage by the Hill equation. The x-axis is shown in a Log scale.

in contrast to a previous report.<sup>7</sup> Moreover, we provide experimental evidence that the RCK1 domain residue E319 together with E487 (corresponding to D362 and E535 of Slo1, respectively) control  $\text{Ca}^{2+}$  sensitivity in SLO-2b, independently of the RCK2 domain. Furthermore, we show that SLO-2 loss-of-function mutations confer resistance to hypoxia in *C. elegans* (contrary to the results by Yuan et al., 2003),<sup>5</sup> while a *slo-1* loss-of-function mutant does not share this phenotype. These results establish the *C. elegans* SLO-2 channels to be functionally more similar to the Slo1 than Slo2 mammalian channels but with important differences from Slo1 channels in the  $\text{Ca}^{2+}$  sensing mechanism.

## Results

**Cloning and expression of the *slo-2b* gene in *Xenopus* oocytes.** The *slo-2* gene in *C. elegans* encodes two protein isoforms. The SLO-2a isoform has been previously described,<sup>7</sup> and here we describe the SLO-2b isoform. SLO-2b is identical to SLO-2a starting from residue R40 of SLO-2a, but its N-terminal end is shorter by 22 and variant in 17 amino acids from SLO-2a. The full-length *slo-2b* gene encodes a 1086 amino acid protein, which is named F08B12.3c, as an alternative splice form of the *C. elegans slo-2* in the Worm database. All amino acids of the SLO-2b from R18 (corresponds to R40 in SLO-2a) are identical to the SLO-2a

amino acids (Fig. 1A). The *slo-2b* cDNA was subcloned into the vector pGEMsh and expressed in *Xenopus* oocytes.<sup>15</sup> Recording from patches in the inside-out patch configuration, using a step protocol from -200 to 200 mV, we found that SLO-2b is a Ca<sup>2+</sup>- and voltage-dependent potassium channel (Fig. 1B). The macroscopic current reached the range of 2–10 nA at 60  $\mu$ M Ca<sup>2+</sup> with 200 mV depolarization in the absence of internal Cl<sup>-</sup>, a finding that differed from previously reported SLO-2a data.<sup>7</sup> To provide estimates of the Ca<sup>2+</sup> dependence of the SLO-2b current regulation, conductance estimates were re-plotted showing the effect of Ca<sup>2+</sup> on conductance at different depolarized potentials (Fig. 1C). Such plots could be fit with the Hill equation with a half maximal activation of the conductance at a voltage range of over 80 mV occurring at [Ca<sup>2+</sup>] concentrations of 10.4 ~ 39.5  $\mu$ M. The Hill coefficients for such relationships ranged from 1.8 to 2.4, suggesting that at least two Ca<sup>2+</sup> ions cooperate to activate SLO-2b.

**The SLO-2b channel has a similar conductance with the SLO-2a channel but is not Cl<sup>-</sup> dependent.** In order to further investigate the effect of Cl<sup>-</sup> on the activation of SLO-2b channels, we performed inside-out patch recordings in symmetrical potassium solutions, either in 160 mM KMES or 160 mM KCl. Plotted normalized G-V curves in different Ca<sup>2+</sup> concentrations established the Ca<sup>2+</sup>-dependent activation of SLO-2b under both conditions (Fig. 2A and B). However, at high Ca<sup>2+</sup> (ranging from 10 ~ 300  $\mu$ M) concentrations and at negative potentials the conductance values were much higher in 160 mM KCl than in 160 mM KMES. Thus, superficially, Cl<sup>-</sup> seemed to increase the activity of the SLO-2b channel. We tested the possibility that Cl<sup>-</sup> activated a conductance independent of SLO-2b in *Xenopus* oocytes by running a ramp protocol on the same patch perfused in its inner surface with either 160 mM KCl or 160 mM KMES (with 160 mM KMES in its outer surface) in 60  $\mu$ M Ca<sup>2+</sup>. The recorded currents obtained by perfusion with 160 mM KCl (Fig. 2C, black line), following offsetting the holding current at 0 mV, showed relatively symmetrical currents (Fig. 2C, solid blue line). This was in contrast to the currents obtained in 160 mM KMES that showed outwardly rectifying currents (Fig. 2C, red line). The difference current between the two conditions (the current recorded in 160 mM KMES subtracted from that recorded in 160 mM KCl) revealed a weak inwardly rectifying current (Fig. 2C, dashed blue line). Uninjected oocytes tested in symmetrical 160 mM NaCl in 60  $\mu$ M Ca<sup>2+</sup>, yielded a weak inwardly rectifying current similar to the difference current obtained in Figure 2C (Fig. 2D, blue line). Almost identical G-V relationships of the two Cl<sup>-</sup>-induced conductances (corresponding to ramp currents shown in the dashed blue trace in Fig. 2C and the solid blue trace in Fig. 2D) indicated that the greater conductance seen in KCl solutions resulted from an oocyte endogenous Ca<sup>2+</sup> activated Cl<sup>-</sup> current that is independent of SLO-2b expression (Fig. 2E and F). Furthermore, we performed experiments to measure and compare the reversal potentials achieved by different concentrations of internal Cl<sup>-</sup> in uninjected versus SLO-2b expressing oocytes. In each Cl<sup>-</sup> concentration we tested, the measured reversal potential values were comparable in the two groups of oocytes and consistent with the predicted value

based on the Nernst Equation for a Cl<sup>-</sup> selective conductance, rather than a K<sup>+</sup> activated one (Fig. S1). Finally, we performed single channel recordings at +100 mV in 0 Ca<sup>2+</sup> with different concentrations of Cl<sup>-</sup>. The data showed no obvious increase in P<sub>o</sub> with elevated Cl<sup>-</sup> concentrations (Fig. 2G and H). This result was in sharp contrast to similar recordings using the Slack channel as a positive control. At -100 mV the Slack P<sub>o</sub> was increased with the elevated Cl<sup>-</sup> concentration (to 30 or 100 mM Cl<sup>-</sup> in 50 mM Na<sup>+</sup>) (Fig. S2). At 1  $\mu$ M Ca<sup>2+</sup> the P<sub>o</sub> of SLO-2b in different Cl<sup>-</sup> concentrations could not be measured because large Cl<sup>-</sup> currents were evoked even in uninjected oocytes. Thus, we obtained inside-out recordings in HEK cells transfected with the cSlo2b cDNA. With 10  $\mu$ M Ca<sup>2+</sup> at 60 mV, P<sub>o</sub> was measured in different Cl<sup>-</sup> concentrations, clearly failing to show P<sub>o</sub> increases with increasing Cl<sup>-</sup> concentrations (Fig. S3A–C). However, the increased Ca<sup>2+</sup> concentration clearly led to a higher P<sub>o</sub> of cSlo2b channels (Fig. S3A–C). These results combined suggest that the SLO-2b channel isoform is not Cl<sup>-</sup> sensitive, in marked contrast to previous results reported for SLO-2a.<sup>7</sup>

In order to further compare SLO-2b to SLO-2a channels, the unitary conductance of SLO-2b was determined (Fig. S4A–B). Although the activation of SLO-2b is voltage dependent, openings can be observed even at strongly hyperpolarized potentials, provided that there is high enough channel expression. The unitary conductance in symmetrical 160 mM KMES was 107  $\pm$  3 pS. This value is consistent with the unitary conductance reported for SLO-2a.<sup>7</sup> The single-channel open probability at 100 mV in 60  $\mu$ M Ca<sup>2+</sup> was calculated to be 0.39  $\pm$  0.02 by measuring and fitting single-channel open and closed events with a Gaussian function (Fig. S4C and D). Thus, since the open probability (P<sub>o</sub>) at 100 mV in 60  $\mu$ M Ca<sup>2+</sup> was about 67% of the maximal P<sub>o</sub> (Fig. 3B, blue dashed line), the maximal P<sub>o</sub> was calculated at around 58%.

**The biophysical properties of SLO-2 channels are closer related to Slo1 than Slo2 channels.** Since SLO-2a and SLO-2b are regulated by Ca<sup>2+</sup> and voltage, we used the Horrigan-Aldrich model aiming to describe the gating behavior of the SLO-2b channel (Fig. S5A). Due to the low open probability of SLO-2b in low Ca<sup>2+</sup> concentrations, we depolarized the membrane to 300 mV. First, at very negative potentials, the SLO-2b voltage sensor is likely to be located in the resting state because the voltage dependence of the SLO-2b channels is weaker than that of the mouse Slo1 (mSlo1) channel.<sup>7</sup> Based on the equation for P(v) (see Materials and Methods, Eqn. 3), Z<sub>L</sub> was given a value of 0.003e, suggesting lack of a voltage dependence. We thus estimated the D value based on the Log(G) vs. V relationship and P(V<sub>max</sub>)/P(V<sub>min</sub>). With some constraints (see Materials and Methods) we could fit all parameters based on Equation 2 (Table 1). The G-V relationship of the wild-type SLO-2b could be fitted well by Equation 2, indicating that the Horrigan-Aldrich model is suitable for describing the properties of SLO-2b (Fig. S5B). Furthermore, the lower value of the SLO-2b Z<sub>j</sub>, compared to that of mSlo1, is consistent with the fact that the voltage sensor of SLO-2b lacks a number of positively charged residues located on its S4 segment. The higher value of the Ca<sup>2+</sup> dissociation constant C reflects the fact that SLO-2b is also less sensitive to Ca<sup>2+</sup>

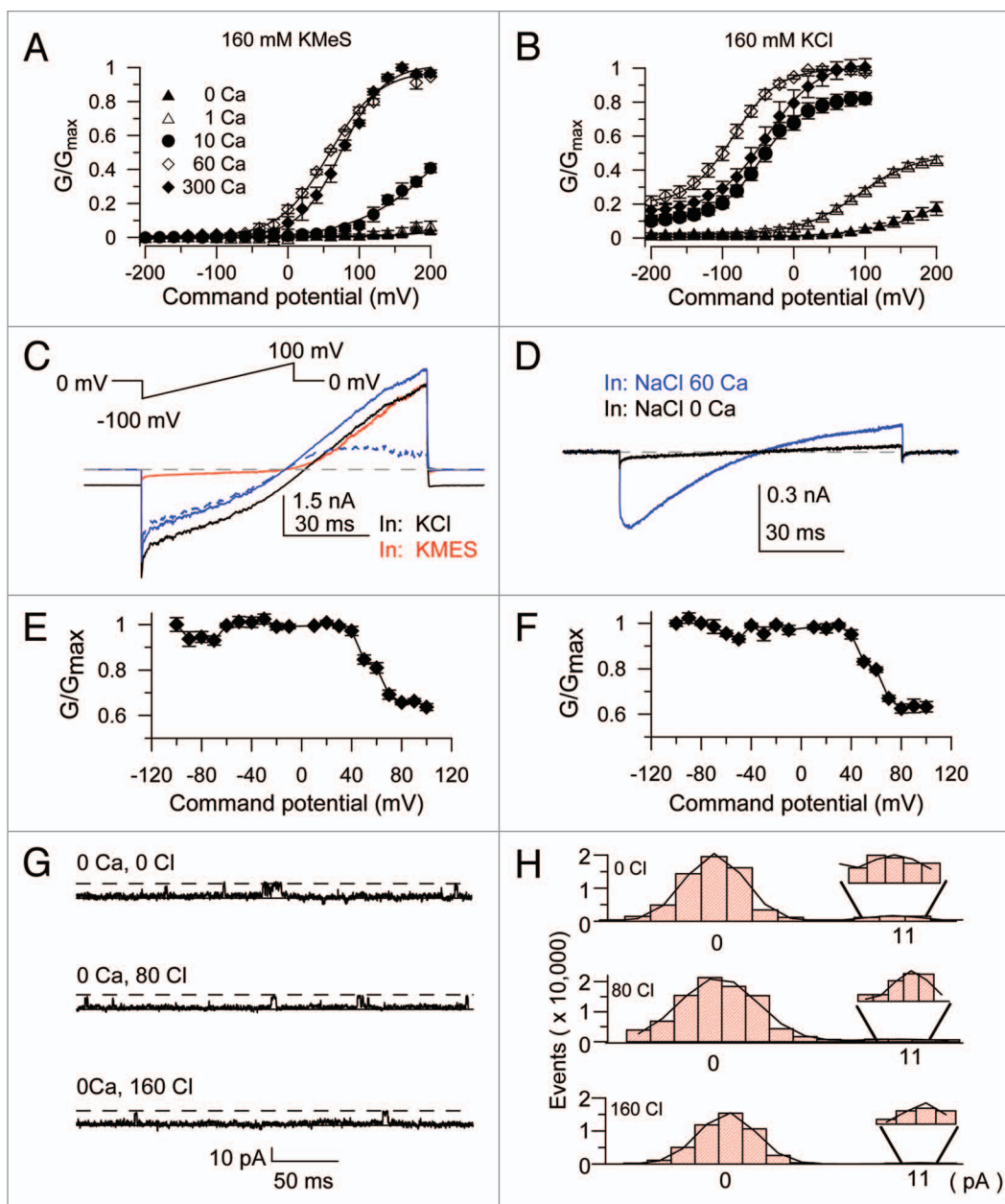


**Figure 2.** SLO-2b currents expressed in *Xenopus* oocytes do not exhibit a dependence on  $\text{Cl}^-$ . (A) Normalized conductances were converted from tail currents recorded in symmetrical 160 mM KMeS bathed in the indicated  $\text{Ca}^{2+}$  concentrations (solutions used are the same as in Fig. 1). (B) Normalized conductances were converted from tail currents recorded in symmetrical 140 mM KCl. Pipette Solution: 140 mM KCl, 20 mM KOH, 10 mM HEPES, 2 mM  $\text{MgCl}_2$ , bath solution contained 140 mM KCl, 20 mM KOH, 10 mM HEPES, 5 mM EGTA with indicated  $\text{Ca}^{2+}$  concentrations. (C) SLO-2b current traces recorded from an inside-out patch with a ramp protocol in symmetrical  $\text{K}^+$  solutions. Pipette Solution: 140 mM KMeS, 20 mM HEPES, 2 mM  $\text{MgCl}_2$ . Black trace was recorded with intracellular 140 mM KCl and 60  $\mu\text{M}$   $\text{Ca}^{2+}$ , the red trace was recorded with 140 mM KMeS and 60  $\mu\text{M}$   $\text{Ca}^{2+}$ . The solid blue trace shows that the holding current was offset. The dashed blue trace indicates the subtraction of the red trace from the solid blue trace (i.e. the  $\text{Cl}^-$ -dependent current). (D) The blue trace (in the presence of  $\text{Ca}^{2+}$ ) shows a current recorded in uninjected oocytes with symmetrical 140 mM NaCl. Pipette Solution: 140 mM NaCl, 20 mM KOH, 10 mM HEPES, 2 mM  $\text{MgCl}_2$ . Bath Solution: 140 mM NaCl, 20 mM KOH, 10 mM HEPES, 5 mM EGTA bathed in either 0  $\mu\text{M}$  or 60  $\mu\text{M}$   $\text{Ca}^{2+}$ . (E and F) Normalized conductances from the dashed blue traces (E) and the solid blue traces (F) that are shown in (C and D). Conductances were normalized to conductance values at  $-100$  mV. (G) The SLO-2b single channel activity was recorded in the inside-out patch configuration with 0  $\text{Ca}^{2+}$  at different  $\text{Cl}^-$  concentrations. Pipette Solution: 140 mM KCl, 20 mM KOH, 10 mM HEPES, 2 mM  $\text{MgCl}_2$  (pH 7.0). Bath Solution: 140 mM KMeS, 20 mM KOH, 10 mM HEPES, 0, 80 or 160 mM Choline Chloride (pH 7.0). (H) The amplitude histogram events in 0, 80 and 160  $\text{Cl}^-$  were fitted with Gaussian functions.

than mSlo1. The G-V of the SLO-2a channel could also be fitted well by the Horrigan-Aldrich model although the parameters used were somewhat different from those for the SLO-2b channels

(see Table 1). The activation time course was well fitted by a single exponential function over the full range of  $\text{Ca}^{2+}$  concentrations (Fig. S5C). The activation time course of the SLO-2b

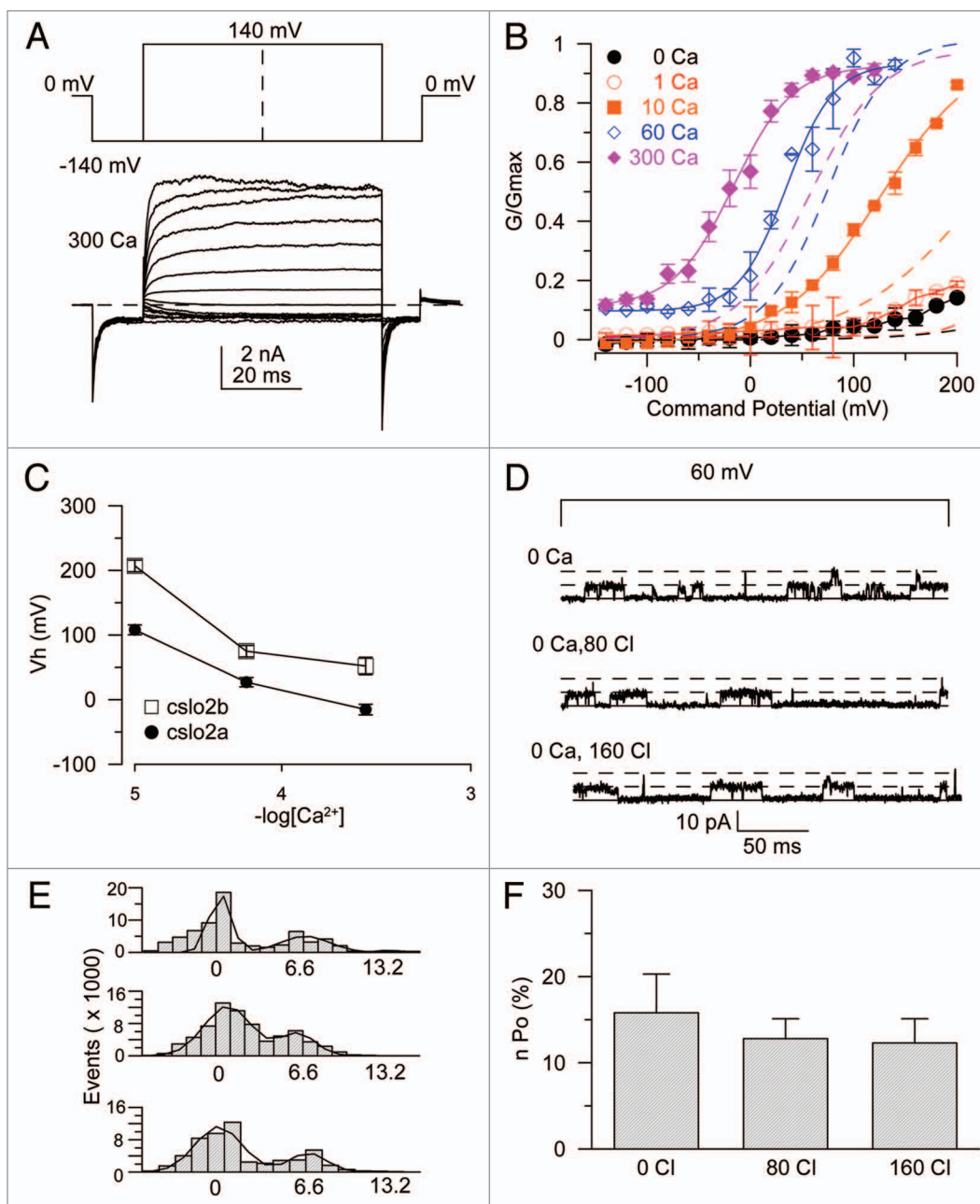


**Figure 3.** SLO-2a is also activated by  $\text{Ca}^{2+}$  but is not sensitive to  $\text{Cl}^-$ . **(A)** Step protocol and current traces recorded from an inside-out patch on oocytes that expressed SLO-2a. Solutions used were the same as in **Figure 1**. **(B)** The G-V curves of SLO-2a are plotted and fitted with a Boltzmann relation. The dashed lines show the fitted G-V curve of SLO-2b. The same  $\text{Ca}^{2+}$  concentrations for SLO-2a and SLO-2b are shown in the same colors. **(C)** Vhs in different  $\text{Ca}^{2+}$  concentrations for the SLO-2a and SLO-2b isoforms. The X-axis is shown in a log scale. **(D)** The single-channel current traces of SLO-2b recorded in the inside-out mode of patch clamp in different  $\text{Cl}^-$  concentrations. **(E)** Amplitude histograms of single-channel activities were plotted and fitted by Gaussian functions. **(F)** The NPo of SLO-2a in different  $\text{Cl}^-$  concentrations were summarized.

is much slower than that of the mSlo1 channel. For SLO-2b, increases in  $\text{Ca}^{2+}$  from 10 to 60  $\mu\text{M}$  produced a 10-fold change in the activation time constant at a given potential (Fig. S5D).

In order to directly compare SLO-2b with SLO-2a, we also performed similar recordings with the SLO-2a isoform. SLO-2a also revealed a large  $\text{Ca}^{2+}$ -dependent current that was insensitive to internal  $\text{Cl}^-$  (Fig. 3A). The conductance versus voltage relationship (G-V) showed that SLO-2a exhibits greater activation at any

given  $\text{Ca}^{2+}$  concentration than SLO-2b (dashed lines for SLO-2b are shown in the same color for a given  $\text{Ca}^{2+}$  concentration). The G-V curve of SLO-2a was left-shifted about 60 mV in each  $\text{Ca}^{2+}$  concentration (Fig. 3B and C). In high  $\text{Ca}^{2+}$  (60–300  $\mu\text{M}$ ), the channel remained in the open state even under highly hyperpolarized conditions (Fig. 3B). These results indicate that the N-terminus of SLO-2a can allosterically regulate channel activity. We further tested whether SLO-2a was sensitive to  $\text{Cl}^-$  by

**Table 1.** Allosteric constants comparing Slo1, Slo3 and SLO-2b activation<sup>4,18</sup>

	Slo1 Horrigan/ Aldrich	Slo3 Zhang/ Lingle	SLO-2b	SLO-2a
L	9.8E-07	1.59E-03	5.29E-07	1.38E-03
Z <sub>Le</sub>	0.3	0.04	→0	→0
J <sub>o</sub>	0.3	0.34	0.05	0.09
Z <sub>je</sub>	0.58	0.34	0.27	0.48
D	25	4.03	30.48	3.83
K <sub>d</sub> ( $\mu$ M)	11	50.16 (H <sup>+</sup> )	48.4	57.8
C	8	0.125	6.57	3.38
E	2.4	0.7	1.37	5.05
V <sub>h</sub>	152	80.1	371	267

measuring the single-channel activity in different Cl<sup>-</sup> concentrations. Our data clearly demonstrate that the P<sub>o</sub> of SLO-2a was insensitive to increasing Cl<sup>-</sup> concentrations (Fig. 3D–F).

The current properties of SLO-2a and SLO-2b seemed to resemble those of mSlo1 but with significant differences. Thus, we investigated whether the Ca<sup>2+</sup> sensing mechanism of SLO-2b was similar to that of mSlo1 channels. Since there is no Ca<sup>2+</sup> bowl in the RCK2 domain of SLO-2b, we focused on the RCK1 high-affinity Ca<sup>2+</sup> binding site. We aligned the SLO-2b (or cslo2) amino acid sequence with that of the Ca<sup>2+</sup>-sensitive mSlo1 and the related but Ca<sup>2+</sup>-insensitive rSlo2 (or slack) (Fig. 4A). The E325 and E487 residues of SLO-2b corresponded to the D367 and E535 of mSlo1, respectively, which have been shown to greatly affect Ca<sup>2+</sup> sensitivity (e.g., 12). We performed alanine scanning mutagenesis on and around these negatively charged residues (Fig. 4E). The E325A mutant did not substantially change the Ca<sup>2+</sup> sensitivity of the SLO-2b channel (Fig. 4C and E). In contrast, the E319A mutant (corresponding to the D362 residue in mSlo1) largely abolished the Ca<sup>2+</sup> sensitivity of the SLO-2b channel (Fig. 4B). The E319D, E319N and E319R mutants also decreased the Ca<sup>2+</sup> sensitivity of SLO-2b (Fig. S6A and B). Similarly, the Ala mutant at position E487, which corresponds to the critical Ca<sup>2+</sup>-sensitive Slo1 residue E535, dramatically decreased Ca<sup>2+</sup> sensitivity of SLO-2b channel activity (Fig. 4D). All other mutants we tested did not substantially change the Ca<sup>2+</sup> sensitivity of the SLO-2b channel, exhibiting V<sub>h</sub> values similar to the wild-type SLO-2b (Fig. 4E). We also tested mutants of the two positive SLO-2b residues (i.e., E319 and E487) at the corresponding SLO-2a channel positions (i.e., E340A and E508A). The results show that these mutations also largely abolished Ca<sup>2+</sup> sensitivity in SLO-2a channels (Fig. S6C and D).

Although the E319A and E487A mutants dramatically decreased the Ca<sup>2+</sup> sensitivity of SLO-2b channels, neither of them alone completely abolished Ca<sup>2+</sup> sensitivity of SLO-2b channels, nor did the double mutant (it showed a similar effect as the single mutants). We thus investigated whether the RCK2 domain of the SLO-2b channels contributed to Ca<sup>2+</sup> sensitivity. Neutralization mutants of the non-conserved negative residues around the residue that corresponds to the Na<sup>+</sup> regulatory site D818 in Slo2.2

were tested for potential effects on Ca<sup>2+</sup> sensitivity. None of the D759N, D763N and the triple mutant E754N/E756N/E757N showed obvious Ca<sup>2+</sup> sensitivity changes (Fig. S6B). We constructed a chimeric channel, in which the entire RCK2 domain of the SLO-2b channel was replaced by the RCK2 domain of the rSlo2.2 (slack) channel, to test the role of the RCK2 domain in Ca<sup>2+</sup> sensing (Fig. 5A). This chimeric channel showed no obvious decrease in Ca<sup>2+</sup> sensitivity. Although the V<sub>h</sub> in 60  $\mu$ M Ca<sup>2+</sup> was right-shifted by 200 mV, the V<sub>h</sub> in 0 Ca was also right-shifted because the G/Gmax in 0 Ca at 300 mV was only 1/3 value of the wild-type SLO-2b (Fig. 5B). Since replacement of the SLO-2b RCK2 domain right-shifted the voltage-dependent activation even in the absence of Ca<sup>2+</sup>, we concluded that it reflected a Ca<sup>2+</sup>-independent effect on channel gating. Also, the RCK2 of Slack did not confer Na<sup>+</sup> sensitivity to the chimeric channel, even though it contained the Na<sup>+</sup> coordination site of Slack suggesting further differences from the Slack channel. Thus, the RCK2 of SLO-2 is likely to contribute less to the Ca<sup>2+</sup>-sensitivity of the channel than the RCK1 domain. Based on the recent crystal structure of the C-terminal domain of hSlo1, we constructed a homology model of SLO-2b. This model shows the E487 and E319 residues within reasonable proximity to be able to coordinate Ca<sup>2+</sup> (Fig. 5C).

We tested if Cd<sup>2+</sup> or Mg<sup>2+</sup> ions could also activate the SLO-2b channel. Cd<sup>2+</sup> has been previously shown to activate mSlo1 channels by binding to the D362 residue, which corresponds to E319A in the SLO-2b channel. However, Cd<sup>2+</sup> could not activate the SLO-2b channel at concentrations up to 200  $\mu$ M (Fig. S7), whereas it does activate the mSlo1 channel at concentrations in the range of tens of micromolar. Mg<sup>2+</sup> activated the SLO-2b channel but less potently than mSlo1 (Fig. 6A). Using a ramp protocol from -100 mV to +100 mV, we obtained the Mg<sup>2+</sup> dose-dependent activation curve. At 100 mV, the current level with 100 mM Mg<sup>2+</sup> in the bath was only 10% of the current level at 300  $\mu$ M Ca<sup>2+</sup> (Fig. 6A). Similarly, Mg<sup>2+</sup> dose-dependent activity could also be observed with increasing voltage steps in the range from 60–200 mV. This activity was higher in bath solutions including 10 mM Mg<sup>2+</sup> compared to 1 mM Mg<sup>2+</sup> but was much lower than at 300  $\mu$ M Ca<sup>2+</sup> (Fig. 6C1–3). The G-V relationship of the Mg<sup>2+</sup> activation for SLO-2b was plotted and fitted with the Boltzmann equation (Fig. 6B), showing an obvious left shift with increasing Mg<sup>2+</sup> concentrations. Next, we determined how the Ca<sup>2+</sup> binding site influences Mg<sup>2+</sup> sensitivity by measuring the activity of the E487A mutant. Since the G-V relationship was largely out of the measurable range, it appears that the E487A only right-shifted the G-V relationship but did not abolish Mg<sup>2+</sup> sensitivity (compare Fig. 6B and D). These results indicate that G-V relationships could be right-shifted by the E487A mutant but that the Mg<sup>2+</sup> sensitivity was maintained. Considering that the E487A also right-shifted the G-V curve at 0  $\mu$ M Ca<sup>2+</sup>, the possibility that an independent Mg<sup>2+</sup> binding site exists cannot be excluded.

**SLO-2 confers sensitivity to hypoxia and functions differently from SLO-1 in *C. elegans*.** SLO-2 channels have previously been reported to have a role in the *C. elegans* response to hypoxia.<sup>5</sup> In this report, worms lacking a functional SLO-2

channel were more sensitive to hypoxia-induced lethality than wild type. Given the similarities of SLO-2 channels to mSlo1, we tested the effects of loss of function in both *slo-2* and *slo-1* on sensitivity to hypoxia in *C. elegans*. To our surprise, when we tested *slo-2* mutant animals in three different paradigms of hypoxia, we found that they were significantly resistant to hypoxia, rather than sensitive. *slo-1*; *slo-2* double mutant animals were also resistant to hypoxia. In contrast, *slo-1* mutants were not different from wild-type strains.

There are several methods for inducing hypoxic responses in the worm, and we used three different approaches to induce hypoxia. First, we incubated the animals with cobalt chloride, which induces expression of the hypoxia inducible transcription factor, HIF-1<sup>16,17</sup> (Fig. 7A). Second, we incubated worms in a bio-bag environmental chamber that uses an oxygen scavenger to remove oxygen from the enclosed environment, which generates O<sub>2</sub> levels well less than 1%,<sup>18,19</sup> as tested by a chemical indicator enclosed in the bag (Fig. 7B). Third, we used a hypoxia chamber similar to the one used previously<sup>5,20</sup> (Fig. 7C). In this chamber, oxygen in the atmosphere is replaced by a gas that is pumped in, and oxygen levels are monitored by a sensor. In our experiments, we maintained the oxygen at 0.1%. Unlike the previous study that used a gas mixture of 5% CO<sub>2</sub>, 10% H<sub>2</sub> and 85% N<sub>2</sub>, we used 100% N<sub>2</sub> gas, as 10% H<sub>2</sub> is flammable. Additionally our experiments were performed at 25°C rather than the 27°C used in the previous study.<sup>5</sup> Regardless of the method used to cause or mimic hypoxia, we found that *slo-2* mutant animals were significantly resistant to hypoxia, whereas *slo-1* mutant animals were not. Loss of function of the SLO-2 channel improved survival under hypoxic conditions, strongly suggesting that *slo-2* confers sensitivity to hypoxia.

## Discussion

We have shown that the *C. elegans* SLO-2b and SLO-2a isoforms are both voltage and Ca<sup>2+</sup>-dependent potassium channels. Neither of these SLO-2 channels exhibits Cl<sup>-</sup> sensitivity, as previously reported for the SLO-2a channel. Thus, the N-terminal amino acid differences could not account for this difference, although the N-terminus of SLO-2 allosterically led to a shift in the G-V relationship. Our results suggest that contamination by an endogenous Cl<sup>-</sup> current present in *Xenopus* oocytes is likely

to have misled the SLO-2a work.<sup>7</sup> Endogenous Cl<sup>-</sup> currents in oocytes have been reported to arise from several Cl<sup>-</sup> channels that can be activated by Ca<sup>2+</sup>.<sup>21-24</sup>

The G-V relationship of the SLO-2b channel could be described well by the Horrigan-Aldrich model, which was developed for describing gating properties of the Slo1 channel. Recently, one crystal structure of the gating ring from the human BK channel in the presence of 50 mM [Ca<sup>2+</sup>]<sub>i</sub> (PDB ID code: 3MT5) revealed that one Ca<sup>2+</sup> ion was coordinated by residues in the Ca<sup>2+</sup> bowl of the RCK2 domain of the Ca<sup>2+</sup>-bound crystal

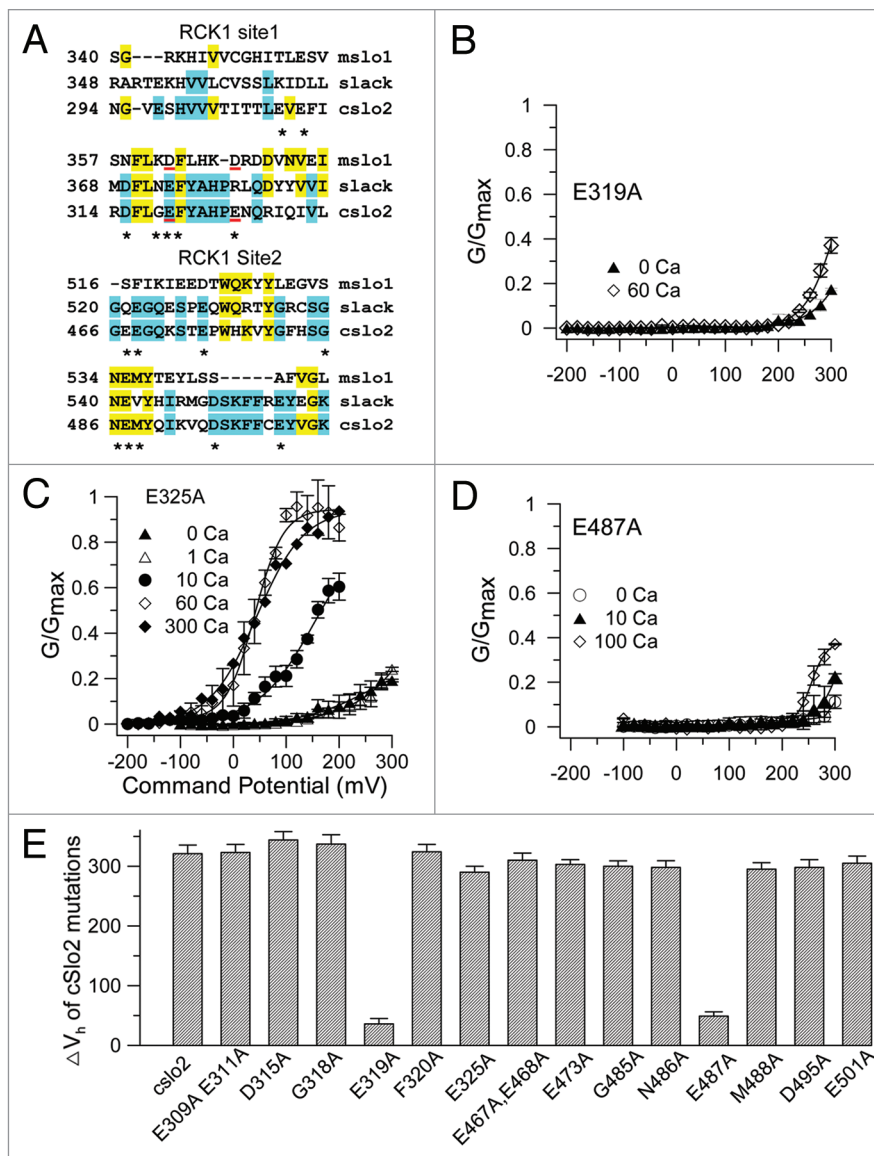


**Figure 4.** Identification of a Ca<sup>2+</sup> binding site in the RCK1 domain of the SLO-2b channel. (A) Alignment of amino acid sequence around the Ca<sup>2+</sup> binding site in RCK1 domain of SLO-2b (indicated as cslo2) channel with the mslo1 and the rat slack channel. \*Denotes the Ala scanned tested mutations. The E325 and E487 residues of SLO-2b correspond to the D367 and E535 residues of mslo1 respectively, which have been suggested to form a Ca<sup>2+</sup> coordination site in Slo1. (B) The G-V curves of E319A mutant are plotted and fitted with a Boltzmann relation. (C and D) The G-V relationships of the E325A and E487A mutants are plotted and fitted with the Boltzmann equation. (E) Effect of individual and combined mutations on Ca<sup>2+</sup> activation. The  $\Delta V_h = V_h$  in 0  $\mu\text{M}$  [Ca<sup>2+</sup>]<sub>i</sub> -  $V_h$  in 60  $\mu\text{M}$  [Ca<sup>2+</sup>].

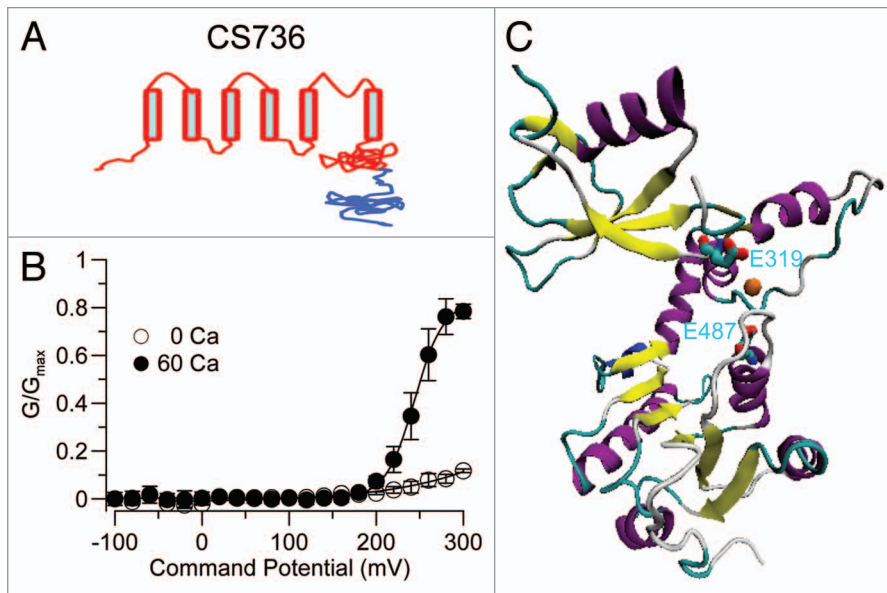


**Figure 5.** The RCK2 domain contributes less to the  $\text{Ca}^{2+}$  sensitivity of SLO-2b than the RCK1 domain. **(A)** The cartoon of a chimera (CS736) between Slack (that is not  $\text{Ca}^{2+}$ -sensitive) and SLO-2b. The RCK2 domain of SLO-2b was replaced by the RCK2 domain of Slack (blue). **(B)** The normalized G-V curve of the CS736 chimera shows a rightward  $V_h$  shift of about 200 mV in both 0 and 60  $\mu\text{M}$  intracellular  $\text{Ca}^{2+}$ . **(C)** An approximation of the  $\text{Ca}^{2+}$  coordination site obtained from the C-terminal homology model of SLO-2b based on the crystal structure of the Slo1 C-terminus (3NAF).

structure, whereas no  $\text{Ca}^{2+}$  was observed in this crystal at the putative RCK1 D367/D362 site.<sup>10</sup> Thus, the  $\text{Ca}^{2+}$  binding site on RCK1 domains is not supported yet by X-ray structural evidence. It has been proposed that neutralization of the D362A/D367A residues prevents  $\text{Ca}^{2+}$ -induced conformational transitions rather than  $\text{Ca}^{2+}$  binding.<sup>13</sup> Alternatively, a recent model from another crystal structure in the absence of  $\text{Ca}^{2+}$  has proposed that D367 and E535 form a  $\text{Ca}^{2+}$  coordination site (PDB ID code: 3NAF).<sup>12</sup> The role of D362/D367 site is also involved in regulating  $\text{Cd}^{2+}$  sensitivity.<sup>2</sup> Interestingly, in the SLO-2b channel, mutation of the E319 residue that corresponds to D362 in mSlo1 did change  $\text{Ca}^{2+}$  sensitivity, in contrast to mutation in the E325 residue that corresponds to D367 in mSlo1 that did not. The E319 site did not sense  $\text{Cd}^{2+}$ . Although it is possible that the change in apparent affinities we have measured results from simply disrupting the transduction of a process regulated by a  $\text{Ca}^{2+}$ -binding site located elsewhere, it is equally possible that in SLO-2b E319 is part of a direct  $\text{Ca}^{2+}$  coordination site. Our homology model of SLO-2b based on hSlo1 as a template localizes E319 adjacent to E487, which corresponds to E535 in Slo1. Our results with the SLO-2b RCK1 domain E319/E487  $\text{Ca}^{2+}$  coordination site support the model proposed for the Slo1 channel corresponding to E535 as being part of the coordination and exchanging the D367 with an equivalent contribution by the D362, which corresponds to E319 in the SLO-2b channel.

Although the SLO-2 amino acid sequence shows greater homology to the Slack channel (40.8% identity) than to the mSlo1 channel (16.3%), the electrophysiological properties of SLO-2 resemble Slo1 more than Slo2 channels. How the

mammalian Slo2 channel evolved to sense  $\text{Na}^+$  instead of  $\text{Ca}^{2+}$  is an intriguing problem that remains to be addressed.

Since the  $K_d$  of the  $\text{Ca}^{2+}$  dependence of SLO-2b and SLO-2a (30 ~ 58  $\mu\text{M}$ ) is significantly higher than mSlo1 (~19  $\mu\text{M}$ ) channels and much above the normal physiological range of  $\text{Ca}^{2+}$  concentrations, it is intriguing to consider how these channels are activated under normal physiological conditions. Clusters of mSlo1 with  $\text{Ca}^{2+}$  channels have been widely reported and local concentrations of free  $\text{Ca}^{2+}$  in chromaffin cells have been reported to elevate  $\text{Ca}^{2+}$  to 60  $\mu\text{M}$ .<sup>25</sup> In *C. elegans*, SLO-2 channels may utilize a similar strategy to sense local  $\text{Ca}^{2+}$  levels. A recent report points out that SLO-2 channels are co-localized and activated by the  $\text{Ca}^{2+}$  channel EGL-19 and play a major role in determining the muscle action potential.<sup>26</sup>

Finally, SLO-2 channels are widely expressed in muscle cells and the cell body of neurons, while the SLO-1 channels are mainly expressed in presynaptic terminals,<sup>7,27</sup> suggesting distinct functions for these SLO channels. The role of potassium channels in hypoxia has been widely studied. The overall dependence of the hypoxic state on potassium channels depends on the type of  $\text{K}^+$  channels and the location of their expression as well as the experimental model used. Excessive  $\text{K}^+$  efflux and intracellular  $\text{K}^+$  depletion had been clearly linked to apoptosis in neurons and other cells during hypoxia.<sup>28-30</sup> Furthermore, both blockers and overexpression of dominant-negative forms of potassium channel subunits in neurons contribute to attenuation of hypoxia-induced apoptosis.<sup>30-32</sup> Consistently, loss of SLO-2 channel function conferred resistance to hypoxia in *C. elegans*, in contrast to previously described effects.<sup>5</sup> This role for loss-of-function of the SLO-2 channel is consistent with the electrophysiological properties and expression pattern of SLO-2 compared to SLO-1 channels, loss-of-function of which failed to show this phenotype. SLO-2 channels have been shown to be involved in mitochondrial potassium transport leading to protection in anesthetic preconditioning but K channel contributions to hypoxic preconditioning remain unclear.<sup>33,34</sup> Taken together, our results provide a revised view of the biophysical characteristics of SLO-2 channels and their relationship to the hypoxic phenotype in *C. elegans*.

## Materials and Methods

**Constructs and mutations.** Genomic and cDNA sequences of slo-2b were obtained from the worm database (www.wormbase.org). The ESTs (1522e1, 1193) of *C. elegans* slo-2 were gifts from Professor Yuji Kohara at the National Institute of Genetics, Mishima, Japan. The 5' 1349 bp of the cDNA sequence of



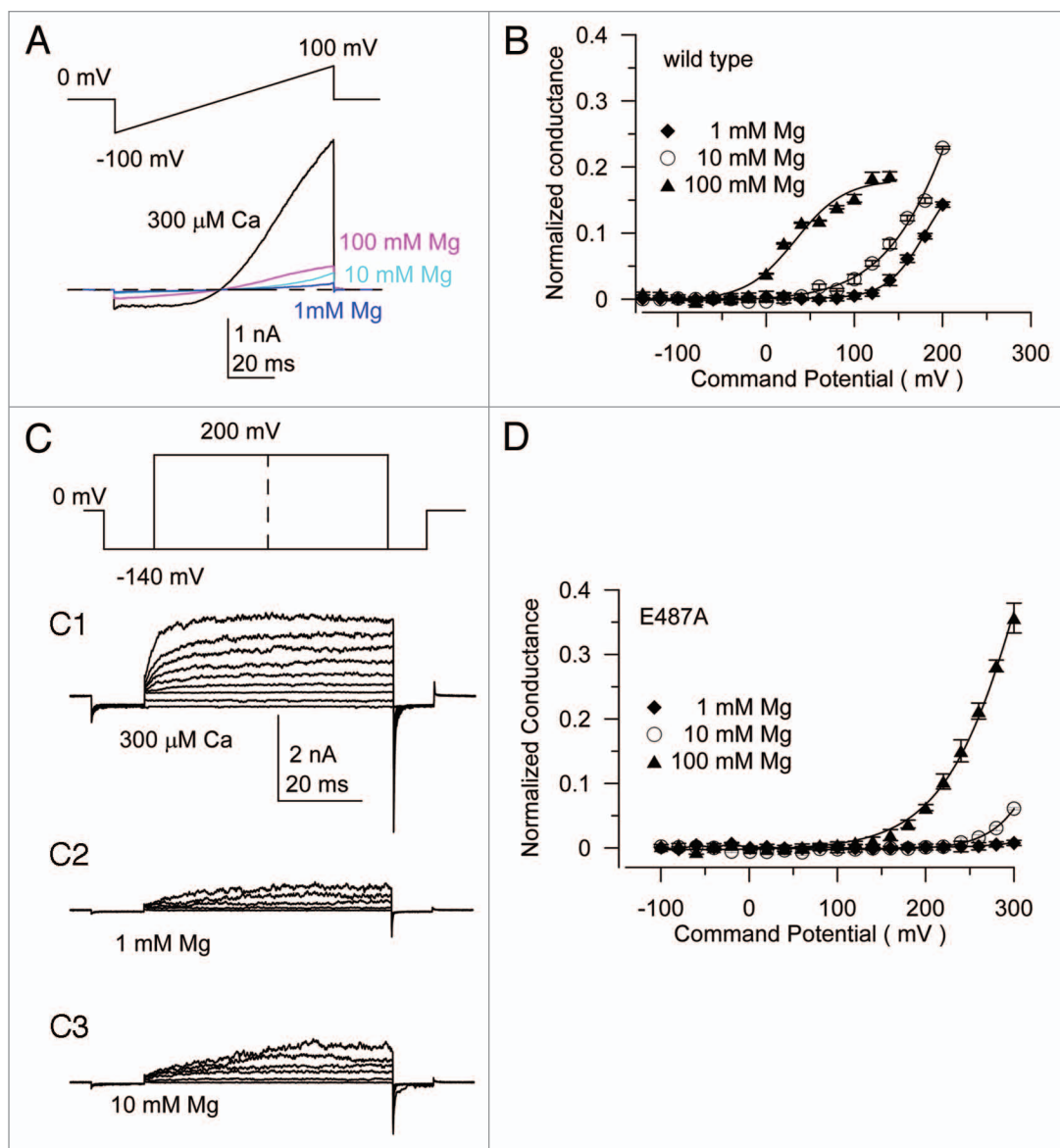


**Figure 6.** Mg<sup>2+</sup> may use an independent binding site to activate SLO-2b with a weaker potency than Ca<sup>2+</sup>. (A) Representative traces with intracellular 300 μM Ca<sup>2+</sup> or indicated concentration of Mg<sup>2+</sup> in a ramp protocol from -100 to +100 mV. (B) Mean G-V relationship of Mg<sup>2+</sup> activation of SLO-2b current summarized from records obtained from the wild-type SLO-2b. (C) Representative traces with intracellular 300 μM Ca<sup>2+</sup> or indicated concentration of Mg<sup>2+</sup> in a voltage step from -140 to +200 mV (C1-C3). (D) Mean G-V relationship of Mg<sup>2+</sup> activation of SLO-2b current summarized from records in E487A mutations.

slo-2b was obtained by PCR from EST clone 1522e1. The primers were flanked with BamHI and XmaI restriction endonuclease sites, at 5' and 3' respectively. This 5' fragment was inserted into the *Xenopus* oocyte expression vector pGEM-sh,<sup>14</sup> using the BamHI and XmaI sites. The nucleotides 1350-1356 of the slo-2b cDNA represent an endogenous XmaI site. A 3' cDNA fragment was isolated by restriction endonuclease digestion from the EST clone 1193 in the pME18S-FL3 vector, using XmaI and XhoI. This fragment was inserted into the 5' fragment-containing pGEM-sh construct that had been digested with XmaI and XhoI, so that the 5' and 3' cDNA fragments were joined together at the XmaI site. The N-terminal 450bp cDNA encoding sequence of slo-2a was synthesized by the GenScripts

Company and flanked by BamHI and NgoMIV endonuclease sites. A NgoMIV endonuclease site mutation was made in the corresponding sequence of slo-2b. Then the corresponding N-terminus of slo-2b constructs was cut from the BamHI/ NgoMIV site and replaced by a synthesized N-terminus of slo-2a. Finally, the inserted NgoMIV endonuclease site was deleted by mutagenesis.

The CS736 chimeras were made by replacing the RCK2 domain of *slo-2b* from amino acid 736 with the Slack RCK2 domain from amino acid 803 to the end of the protein. Mutants were made following previously published procedures.<sup>35</sup>

**Oocyte isolation and culture.** Stage VI oocytes from female *Xenopus laevis* frogs were harvested and used for cRNA injection,

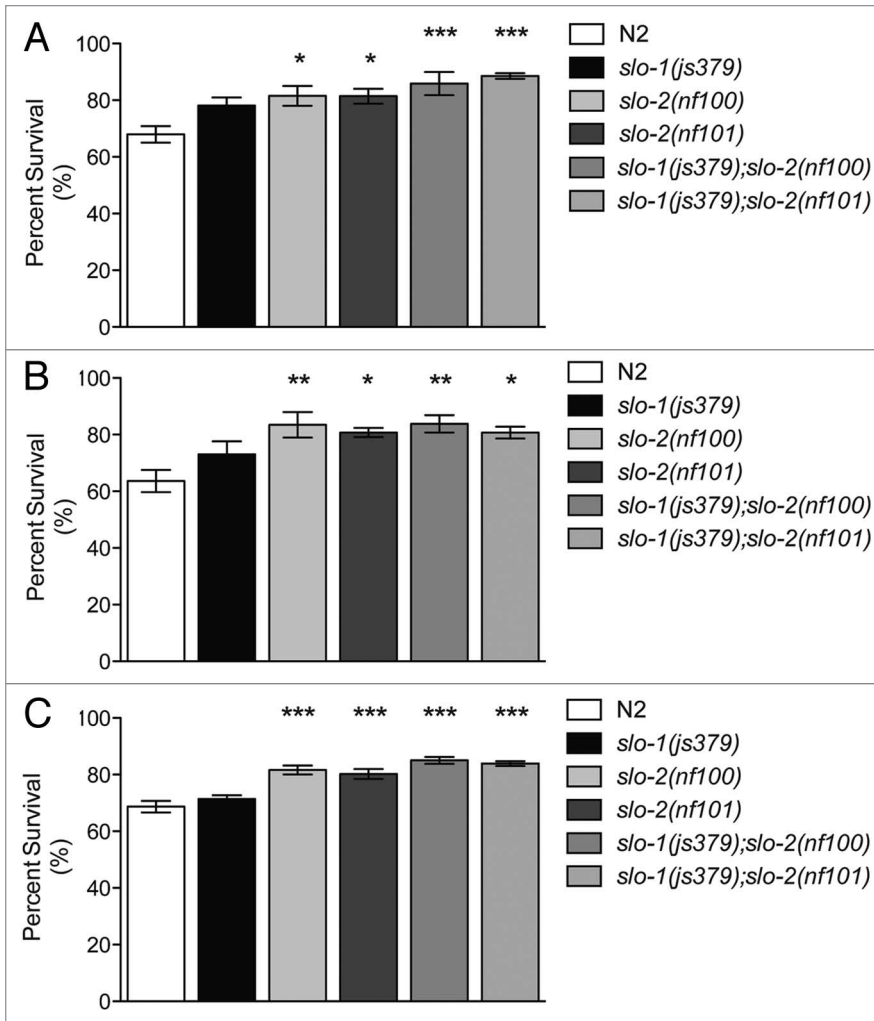


**Figure 7.** *slo-2* mutant animals are resistant to severe hypoxia-induced death. Hypoxic responses were induced in three different paradigms. Severe hypoxia is defined as < 0.3% oxygen. (A) Cobalt chloride was used to induce hypoxia-inducible factor (HIF-1) signaling without altering atmospheric oxygen levels ( $n = 6$ ). (B) Animals were exposed to < 1% oxygen for 8 h at 27°C in a Bio-bag environmental chamber ( $n = 5$ ), and (C) Animals were exposed to 0.1% oxygen for 16 h in a hypoxia chamber ( $n = 6$ ). In each case, *slo-2(nf100)* and *slo-2(nf101)* mutant animals are significantly resistant to hypoxia induced death relative to wild-type N2. Loss of *slo-1* did not confer resistance to hypoxia-induced death. *slo-1(js379);slo-2(nf100)* and *slo-1(js379);slo-2(nf101)* double mutant animals are significantly resistant to hypoxia induced death compared with N2 or the *slo-1(js379)* single mutant. Error bars are s.e.m. For indicated comparisons: \* $p < 0.05$ ; \*\* $p < 0.01$ ; \*\*\* $p < 0.001$ .

as previously described.<sup>36,37</sup> Each oocyte was injected with 50 nl of ~1  $\mu\text{g}/\mu\text{l}$  concentration of cRNA. Currents were recorded within 3–5 d.

**HEK293 cell culture and transfection.** The HEK293 cells were cultured on coverslips that sunk in the diameter 36 mm dish in DMEM culture medium. The SLO-2b were cloned into pcDNA3 vector and transfected 24–48 h before recording by following the Invitrogen lipofectamine transfection protocol.

**Electrophysiology.** Currents were recorded in the inside-out patch configuration, using an EPC 9 amplifier (HEKA) and the Pulse fit program (HEKA). Single-channel analysis followed

previously described procedures.<sup>14</sup> Each series of  $G/V$  curves were obtained from the same patch, and conductances were normalized to estimates of maximal fitted conductance obtained with 60  $\mu\text{M}$   $\text{Ca}^{2+}$ . Individual  $G/V$  curves were fitted with a Boltzmann function of the following form:

$$G(V) = \frac{G_{\max}}{1 + \exp\left(\frac{-zF(V-V_b)}{RT}\right)}$$

Eqn. 1

where  $G_{\max}$  is the fitted value for maximal conductance at a given  $\text{Ca}^{2+}$  concentration.  $V_b$  is the voltage of half maximal activation of conductance, and  $z$  reflects the net charge moved across the membrane during the transition from the closed to the open state.  $\Delta V_b = V_h$  at 0–100  $\mu\text{M}$   $[\text{Ca}^{2+}]_i$ .

**Allosteric models of activation of BK channels.** The  $\text{Ca}^{2+}$  and voltage dependence of activation of the SLO-2b channels and SLO-2a could be reasonably well described by the Horrigan-Aldrich model that was developed for Slo1 channels.<sup>38</sup> For the scheme used here (Fig. S5A), we assumed that the effects of  $\text{Ca}^{2+}$  involved a single  $\text{Ca}^{2+}$ -dependent equilibrium occurring with each of the four subunits. The system was described by three relatively independent equilibrium constants:  $L$  indicates the intrinsic equilibrium constant for the close-open transition;  $J$  defines the equilibrium constant for the voltage sensor moving between resting and activation states;  $K$  defines the equilibrium constant for interaction with  $\text{Ca}^{2+}$ . In turn, each process was allosterically coupled to the other two processes by coupling constants.  $D$  defines the coupling between voltage sensor movement and channel opening;  $C$  defines the coupling between  $\text{Ca}^{2+}$  binding and channel opening;  $E$  defines the coupling between  $\text{Ca}^{2+}$  and voltage sensor movement. The open probability was determined by the equation:

$$P(V, [\text{Ca}]) = \frac{1}{1 + \frac{1}{L} \left[ \frac{1+K+J+KJE}{1+KC+JD+KCJDE} \right]^4}$$

Eqn. 2

where  $L = L(0) \cdot \exp(Z_L V/kT)$ ,  $J = J(0) \cdot \exp(Z_J V/kT)$ ,  $K = [\text{Ca}^{2+}]/K_d$ , where  $K_d$  is the dissociation constant of free  $\text{Ca}^{2+}$ . Hence, at very negative potentials lower than -100 mV and at all  $\text{Ca}^{2+}$  concentrations, the normalized conductance is  $< 0.01$ ,  $(1 + K)^4 \gg L(1 + KC)^4$ . The equation that is used to define  $Z_L$  can be simplified as:

$$P(V) = L(0) \exp\left(\frac{Z_L F V}{RT}\right)$$

### Eqn. 3

Detailed information regarding the Horrigan-Aldrich model has been previously described.<sup>4,38</sup> Some parameters were constrained ( $0 < L < 1$ ,  $0 < Z_L < 10$ ,  $0 < D < 100$ ,  $0 < C < 100$ ) when the G-V was fitted with Eqn. 2.

**C. elegans methods.** Nematode Culture and Strains. *C. elegans* were maintained using standard methods.<sup>39</sup> Strains used were N2 (var. Bristol), *slo-1(js379)*, *slo-2(nf100)*, *slo-2(nf101)*, *slo-1(js379);slo-2(nf100)* and *slo-1(js379);slo-2(nf101)*.

**Assays of severe hypoxia. Cobalt chloride treatment.** Healthy age matched first day adult animals were used. Five hundred microliters of filter sterilized 100 mM cobalt chloride (Acros Organics) was added to 3-d-old Nematode Growth Media (NGM) plates. Plates were seeded with OP50 bacteria 24 h before addition of cobalt chloride. Fifty animals were incubated on plates for 16 h at 20°C (for each 50 worm experiment  $n = 1$ ). Worms were moved to new NGM plates and scored for survival after 24 h. A 1-way analysis of variance (ANOVA) was performed with a significance value of  $p < 0.05$  with Bonferroni's post hoc test comparing each mutant strain to N2.

**Environmental chamber.** Healthy age matched first day adult animals were used. Fifty animals on NGM plates seeded with OP50 were placed in Bio-Bag Environmental Chamber Type A (Becton, Dickinson and Company). Animals were exposed to oxygen levels of less than 1% for 8 h at 27°C, then removed from the bag and moved to new NGM plates and incubated in room atmosphere at 20°C. Survival was scored after 24 h. A 1-way analysis of variance (ANOVA) was performed with a significance value of  $p < 0.05$  with Bonferroni's post hoc test comparing each mutant strain to N2.

**Hypoxic Cabinet:** Healthy age matched second day adult animals were used. Animals were washed with 1 mL of M9 buffer into 1.5 mL polypropylene tubes. The M9 was replaced three times

with 1 mL of M9 that had been bubbled for 30 min with 100% nitrogen gas. Worms were incubated in a Hypoxic Cabinet with an oxygen controller (Coy Laboratory Products) in a final volume of 100  $\mu$ L of M9 at an oxygen level of 0.1% for 16 h at 25°C. Animals were removed from the chamber and moved to new NGM plates and incubated in room atmosphere at 20°C. Survival was scored 24 h after incubation. A 1-way analysis of variance (ANOVA) was performed with a significance value of  $p < 0.05$  with Bonferroni's post hoc test comparing each mutant strain to N2.

**Reagents.** KMES, potassium methanesulphonate; KOH, potassium hydroxide; HEPES, 4-(2-hydroxyethyl)-1-piperazineethanesulfonic acid; MgCl<sub>2</sub>, magnesium chloride; EGTA, ethylene glycol tetraacetic acid; HEDTA, N-(hydroxyethyl)-ethylenediaminetriacetic acid were all purchased from Sigma-Aldrich.

### Disclosure of Potential Conflicts of Interest

No potential conflicts of interest were disclosed.

### Acknowledgments

Z.Z. was supported by American Heart Association Grant 09SDG2290002. D.E.L. was supported by National Institutes of Health Grants R01HL059949 and R01HL090882. J.T.A, A.G.D. and J.C.B were supported by R01AA016837 to J.C.B. We are thankful to Heikki Vaananen and Sophia Gruszecki for isolation of *Xenopus* oocytes, Professor Yuji Kohara for EST clones, Keith Baker and Divya Padmanabha for advice and use of their hypoxia chamber, Leon Avery and the *Caenorhabditis* Genetics Center for *C. elegans* strains and Christopher Lingle, Leon Avery and members of the Logothetis laboratory for helpful discussions and comments on the manuscript and throughout this project.

### Supplemental Material

Supplemental materials may be found here:

<http://www.landesbioscience.com/journals/channels/article/24492>

### References

- Butler A, Tsunoda S, McCobb DP, Wei A, Salkoff L. mSlo, a complex mouse gene encoding "maxi" calcium-activated potassium channels. *Science* 1993; 261:221-4; PMID:7687074; <http://dx.doi.org/10.1126/science.7687074>
- Zeng XH, Xia XM, Lingle CJ. Divalent cation sensitivity of BK channel activation supports the existence of three distinct binding sites. *J Gen Physiol* 2005; 125:273-86; PMID:15738049; <http://dx.doi.org/10.1085/jgp.200409239>
- Schreiber M, Wei A, Yuan A, Gaut J, Saito M, Salkoff L. Slo3, a novel pH-sensitive K<sup>+</sup> channel from mammalian spermatocytes. *J Biol Chem* 1998; 273:3509-16; PMID:9452476; <http://dx.doi.org/10.1074/jbc.273.6.3509>
- Zhang X, Zeng X, Lingle CJ. Slo3 K<sup>+</sup> channels: voltage and pH dependence of macroscopic currents. *J Gen Physiol* 2006; 128:317-36; PMID:16940555; <http://dx.doi.org/10.1085/jgp.200609552>
- Yuan A, Santi CM, Wei A, Wang ZW, Pollak K, Nonet M, et al. The sodium-activated potassium channel is encoded by a member of the Slo gene family. *Neuron* 2003; 37:765-73; PMID:12628167; [http://dx.doi.org/10.1016/S0896-6273\(03\)00096-5](http://dx.doi.org/10.1016/S0896-6273(03)00096-5)
- Bhattacharjee A, Kaczmarek LK. For K<sup>+</sup> channels, Na<sup>+</sup> is the new Ca<sup>2+</sup>. *Trends Neurosci* 2005; 28:422-8; PMID:15979166; <http://dx.doi.org/10.1016/j.tins.2005.06.003>
- Yuan A, Dourado M, Butler A, Walton N, Wei A, Salkoff L. SLO-2, a K<sup>+</sup> channel with an unusual Cl<sup>-</sup> dependence. *Nat Neurosci* 2000; 3:771-9; PMID:10903569; <http://dx.doi.org/10.1038/77670>
- Schreiber M, Salkoff L. A novel calcium-sensing domain in the BK channel. *Biophys J* 1997; 73:1355-63; PMID:9284303; [http://dx.doi.org/10.1016/S0006-3495\(97\)78168-2](http://dx.doi.org/10.1016/S0006-3495(97)78168-2)
- Xia XM, Zeng X, Lingle CJ. Multiple regulatory sites in large-conductance calcium-activated potassium channels. *Nature* 2002; 418:880-4; PMID:12192411; <http://dx.doi.org/10.1038/nature00956>
- Yuan P, Leonetti MD, Pico AR, Hsiung Y, MacKinnon R. Structure of the human BK channel Ca<sup>2+</sup>-activation apparatus at 3.0 Å resolution. *Science* 2010; 329:182-6; PMID:20508092; <http://dx.doi.org/10.1126/science.1190414>
- Wu Y, Yang Y, Ye S, Jiang Y. Structure of the gating ring from the human large-conductance Ca(2+)-gated K(+) channel. *Nature* 2010; 466:393-7; PMID:20574420; <http://dx.doi.org/10.1038/nature09252>
- Zhang G, Huang SY, Yang J, Shi J, Yang X, Moller A, et al. Ion sensing in the RCK1 domain of BK channels. *Proc Natl Acad Sci U S A* 2010; 107:18700-5; PMID:20937866; <http://dx.doi.org/10.1073/pnas.1010124107>
- Yusifov T, Javaherian AD, Pantazis A, Gandhi CS, Olcese R. The RCK1 domain of the human BKCa channel transduces Ca<sup>2+</sup> binding into structural rearrangements. *J Gen Physiol* 2010; 136:189-202; PMID:20624858; <http://dx.doi.org/10.1085/jgp.200910374>
- Zhang Z, Rosenhouse-Dantsker A, Tang QY, Noskov S, Logothetis DE. The RCK2 domain uses a coordination site present in Kir channels to confer sodium sensitivity to Slo2.2 channels. *J Neurosci* 2010; 30:7554-62; PMID:20519529; <http://dx.doi.org/10.1523/JNEUROSCI.0525-10.2010>
- Tang QY, Zhang Z, Xia J, Ren D, Logothetis DE. Phosphatidylinositol 4,5-bisphosphate activates Slo3 currents and its hydrolysis underlies the epidermal growth factor-induced current inhibition. *J Biol Chem* 2010; 285:19259-66; PMID:20392696; <http://dx.doi.org/10.1074/jbc.M109.100156>

16. Ho VT, Bunn HF. Effects of transition metals on the expression of the erythropoietin gene: further evidence that the oxygen sensor is a heme protein. *Biochem Biophys Res Commun* 1996; 223:175-80; PMID:8660366; <http://dx.doi.org/10.1006/bbrc.1996.0865>
17. Epstein AC, Gleadle JM, McNeill LA, Hewitson KS, O'Rourke J, Mole DR, et al. *C. elegans* EGL-9 and mammalian homologs define a family of dioxygenases that regulate HIF by prolyl hydroxylation. *Cell* 2001; 107:43-54; PMID:11595184; [http://dx.doi.org/10.1016/S0092-8674\(01\)00507-4](http://dx.doi.org/10.1016/S0092-8674(01)00507-4)
18. Hajeri VA, Trejo J, Padilla PA. Characterization of sub-nuclear changes in *Caenorhabditis elegans* embryos exposed to brief, intermediate and long-term anoxia to analyze anoxia-induced cell cycle arrest. *BMC Cell Biol* 2005; 6:47; PMID:16368008; <http://dx.doi.org/10.1186/1471-2121-6-47>
19. Padilla PA, Nystul TG, Zager RA, Johnson AC, Roth MB. Dephosphorylation of cell cycle-regulated proteins correlates with anoxia-induced suspended animation in *Caenorhabditis elegans*. *Mol Biol Cell* 2002; 13:1473-83; PMID:12006646; <http://dx.doi.org/10.1091/mbc.01-12-0594>
20. Park EC, Ghose P, Shao Z, Ye Q, Kang L, Xu XZ, et al. Hypoxia regulates glutamate receptor trafficking through an HIF-independent mechanism. *EMBO J* 2012; 31:1379-93; PMID:22252129; <http://dx.doi.org/10.1038/emboj.2011.499>
21. Huang F, Rock JR, Harfe BD, Cheng T, Huang X, Jan YN, et al. Studies on expression and function of the TMEM16A calcium-activated chloride channel. *Proc Natl Acad Sci U S A* 2009; 106:21413-8; PMID:19965375; <http://dx.doi.org/10.1073/pnas.0911935106>
22. Schroeder BC, Cheng T, Jan YN, Jan LY. Expression cloning of TMEM16A as a calcium-activated chloride channel subunit. *Cell* 2008; 134:1019-29; PMID:18805094; <http://dx.doi.org/10.1016/j.cell.2008.09.003>
23. Tsunenari T, Sun H, Williams J, Cahill H, Smallwood P, Yau KW, et al. Structure-function analysis of the bestrophin family of anion channels. *J Biol Chem* 2003; 278:41114-25; PMID:12907679; <http://dx.doi.org/10.1074/jbc.M306150200>
24. Qu Z, Wei RW, Mann W, Hartzell HC. Two bestrophins cloned from *Xenopus laevis* oocytes express Ca(2+)-activated Cl(-) currents. *J Biol Chem* 2003; 278:49563-72; PMID:12939260; <http://dx.doi.org/10.1074/jbc.M308414200>
25. Prakriya M, Solaro CR, Lingle CJ. [Ca2+]i elevations detected by BK channels during Ca2+ influx and muscarine-mediated release of Ca2+ from intracellular stores in rat chromaffin cells. *J Neurosci* 1996; 16:4344-59; PMID:8699245
26. Liu P, Ge Q, Chen B, Salkoff L, Kotlikoff MI, Wang ZW. Genetic dissection of ion currents underlying all-or-none action potentials in *C. elegans* body-wall muscle cells. *J Physiol* 2011; 589:101-17; PMID:21059759; <http://dx.doi.org/10.1113/jphysiol.2010.200683>
27. Wang ZW, Saifee O, Nonet ML, Salkoff L. SLO-1 potassium channels control quantal content of neurotransmitter release at the *C. elegans* neuromuscular junction. *Neuron* 2001; 32:867-81; PMID:11738032; [http://dx.doi.org/10.1016/S0896-6273\(01\)00522-0](http://dx.doi.org/10.1016/S0896-6273(01)00522-0)
28. Linnik MD, Zobrist RH, Hatfield MD. Evidence supporting a role for programmed cell death in focal cerebral ischemia in rats. *Stroke* 1993; 24:2002-8, discussion 2008-9; PMID:8248983; <http://dx.doi.org/10.1161/01.STR.24.12.2002>
29. Reeves WB, Shah SV. Activation of potassium channels contributes to hypoxic injury in proximal tubules. *J Clin Invest* 1994; 94:2289-94; PMID:7989584; <http://dx.doi.org/10.1172/JCI117592>
30. Yu SP, Yeh CH, Sensi SL, Gwag BJ, Canzoniero LM, Farhangrazi ZS, et al. Mediation of neuronal apoptosis by enhancement of outward potassium current. *Science* 1997; 278:114-7; PMID:9311914; <http://dx.doi.org/10.1126/science.278.5335.114>
31. Pal S, Hartnett KA, Nerbonne JM, Levitan ES, Aizenman E. Mediation of neuronal apoptosis by Kv2.1-encoded potassium channels. *J Neurosci* 2003; 23:4798-802; PMID:12832499
32. Wei L, Yu SP, Gottron F, Snider BJ, Zipfel GJ, Choi DW. Potassium channel blockers attenuate hypoxia- and ischemia-induced neuronal death in vitro and in vivo. *Stroke* 2003; 34:1281-6; PMID:12677023; <http://dx.doi.org/10.1161/01.STR.0000065828.18661.FE>
33. Wojtovich AP, Sherman TA, Nadtochiy SM, Urciuoli WR, Brookes PS, Nehrke K. SLO-2 is cytoprotective and contributes to mitochondrial potassium transport. *PLoS One* 2011; 6:e28287; PMID:22145034; <http://dx.doi.org/10.1371/journal.pone.0028287>
34. Wojtovich AP, DiStefano P, Sherman T, Brookes PS, Nehrke K. Mitochondrial ATP-sensitive potassium channel activity and hypoxic preconditioning are independent of an inwardly rectifying potassium channel subunit in *Caenorhabditis elegans*. *FEBS Lett* 2012; 586:428-34; PMID:22281198; <http://dx.doi.org/10.1016/j.febslet.2012.01.021>
35. Zhang Z, Zhou Y, Ding JR, Xia XM, Lingle CJ. A limited access compartment between the pore domain and cytosolic domain of the BK channel. *J Neurosci* 2006; 26:11833-43; PMID:17108156; <http://dx.doi.org/10.1523/JNEUROSCI.3812-06.2006>
36. Zhang Z, Zeng XH, Xia XM, Lingle CJ. N-terminal inactivation domains of beta subunits are protected from trypsin digestion by binding within the antechamber of BK channels. *J Gen Physiol* 2009; 133:263-82; PMID:19237592; <http://dx.doi.org/10.1085/jgp.200810079>
37. Jin T, Peng L, Mirshahi T, Rohacs T, Chan KW, Sanchez R, et al. The (beta)gamma subunits of G proteins gate a K(+) channel by pivoted bending of a transmembrane segment. *Mol Cell* 2002; 10:469-81; PMID:12408817; [http://dx.doi.org/10.1016/S1097-2765\(02\)00659-7](http://dx.doi.org/10.1016/S1097-2765(02)00659-7)
38. Horrigan FT, Aldrich RW. Coupling between voltage sensor activation, Ca2+ binding and channel opening in large conductance (BK) potassium channels. *J Gen Physiol* 2002; 120:267-305; PMID:12198087; <http://dx.doi.org/10.1085/jgp.20028605>
39. Brenner S. The genetics of *Caenorhabditis elegans*. *Genetics* 1974; 77:71-94; PMID:4366476